JOURNAL OF GEOPHYSICAL RESEARCH, VOL. 113, C02005, doi:10.1029/2007JC004106, 2008

A model-dye comparison experiment in the tidal mixing front zone on the southern flank of Georges Bank

Changsheng Chen,[1] Qichun Xu,[1] Robert Houghton,[2] and Robert C. Beardsley[3]

Received 15 January 2007; revised 8 June 2007; accepted 30 October 2007; published 9 February 2008.

[1] A process-oriented model-dye comparison experiment was conducted to examine the ability of a numerical ocean model to simulate the observed movement of dye across the tidal mixing front on the southern flank of Georges Bank during 22–26 May 1999. The experiment was made using the unstructured-grid Finite-Volume Coastal Ocean Model (FVCOM) with varying horizontal resolution. The results indicate that the observed cross-isobath movement of the dye patch was primarily controlled by meso-scale temporal and spatial variability of the water temperature and salinity fields. Onset of vertical stratification tended to slow down an upward stretching of the dye column and trapped the dye within the bottom mixed layer. To reach a convergent numerical solution that reproduced the observed lateral turbulent dispersion of dye, the FVCOM grid required a horizontal resolution of ~500 m in the dye study region. Within the tidal mixing front of Georges Bank, the movement of the center of the dye patch was mainly driven by the ensemble velocity integrated over the dye volume, with a first-order contribution from vertical shear of the dye's horizontal velocity.

Citation: Chen, C., Q. Xu, R. Houghton, and R. C. Beardsley (2008), A model-dye comparison experiment in the tidal mixing front zone on the southern flank of Georges Bank, *J. Geophys. Res.*, *113*, C02005, doi:10.1029/2007JC004106.

1. Introduction

[2] One objective of the US GLOBal ECosystem (GLOBEC) Northwest Atlantic/Georges Bank (GB) Program is to examine the physical processes controlling cross-frontal water exchange over GB (Figure 1). The tidal mixing front, characterized by a sharp cross-isobath gradient of water temperature near the ~40-m isobath on the northern flank and ~40 to 60-m isobaths over the eastern and southern flanks in late spring/summer, is generally thought to act as a physical barrier to restrict the flux of nutrients from the stratified regions over the flanks to the mixed region on the crest and thus limit primary productivity over the crest during summer. Since the nutrients decrease rapidly after the spring bloom that occurs in late winter or early spring [*Townsend and Thomas*, 2002], it is essential to understand how nutrients can be transported into the mixed region after the tidal mixing front has been established in late spring/summer. This leads to a key question: what are the physical processes controlling cross-frontal transport of water and tracer over the southern flank tidal front?

[3] Physical processes thought to be important in cross-frontal water transport have been studied as part of the GLOBEC/GB program since its inception in 1992. By tracking fluid particles in a tidally driven 3-D homogenous flow field, *Loder et al.* [1997] found that the Stokes' drift, which is the same order of magnitude as the Eulerian residual flow, leads to an on-bank water movement near the bottom of GB. For the tidal mixing front in summer stratification conditions, *Chen and Beardsley* [1998] found from a 2-D Lagrangian particle tracking experiment that the water in the bottom mixed layer tends to advect upward within the frontal zone, with a small portion of this water near the bottom being transported across the front. The near-bottom cross-bank Lagrangian velocity is about 1–2 cm/s on the southern flank and about 2–4 cm/s on the northern flank. *Pringle and Franks* [2001] derived an analytical solution of a simple tidally induced bottom boundary layer and argued that the cross-frontal water transport can be driven by an asymmetric feature of tidal mixing over tidal cycles. This mechanism was supported by *Chen and Beardsley* [2002] through an alternative analytical solution for an idealized frontal system. The physical mechanisms identified in these 2-D experiments for tidally induced cross-frontal water transport are still valid in 3-D experiments with stratification except that the on-bank movement of fluid particles can be more complex in the 3-D case due to local bathymetry [*Chen et al.*, 2003a, 2003b].

[4] As part of the 1999 GLOBEC/GB Cross-frontal Exchange Processes Study, *Houghton* [2002] conducted several dye tracer experiments on GB in late May and early June to obtain quantitative estimates of on-bank diapycnal Lagrangian water flow in the tidal mixing frontal zone. A

[1]Department of Fisheries Oceanography, School for Marine Science and Technology, University of Massachusetts-Dartmouth, New Bedford, Massachusetts, USA.
[2]Lamont Doherty Earth Observatory of Columbia University, Palisades, New York, USA.
[3]Department of Physical Oceanography, Woods Hole Oceanographic Institution, Woods Hole, Massachusetts, USA.

0148-0227/08/2007JC004106$09.00

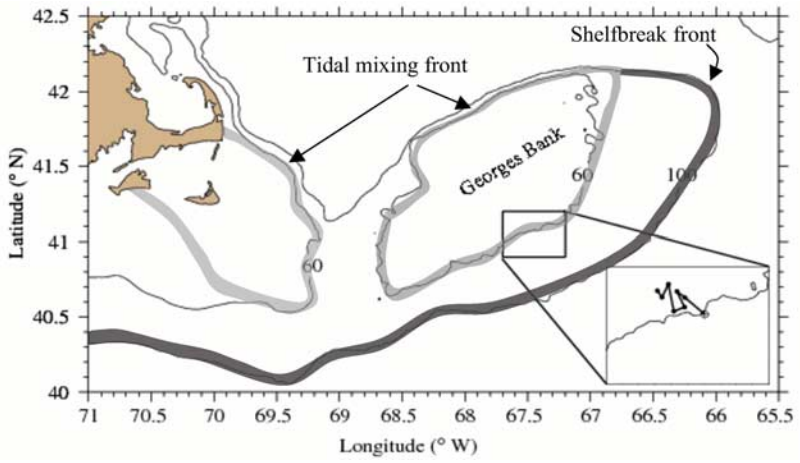

Figure 1. Location of the May 1999 dye study area on the southern flank of Georges Bank. The dye was injected and tracked in the area bounded by the box shown in the figure. The segmented line shown in the lower-right corner is the trajectory of the center of the dye patch estimated using a sequence of dye measurement surveys adjusted empirically in location to the center time of each survey. ⊗: the location of the dye injection and ●: the location of the center dye estimated by subsequent patch surveys.

fluorescent dye was injected into the bottom mixed layer within the frontal zone on both southern and northeastern flanks and then tracked over a period of 4 and 2.5 days respectively using a towed undulating sensor system equipped with a fluorometer and CTD. Significant temporal and spatial variability in water temperature and salinity was observed around the dye patch during each experiment, evidence that the dye patch was part of an evolving mesoscale circulation. As a result, the observed motion of the dye patch and estimates of diapycnal water transport from each experiment represents just one realization of the summer frontal conditions.

[5] In spite of this limitation, however, the dye measurements of *Houghton* [2002] made on GB were the first to provide a direct 3-D view of the cross-frontal Lagrangian water movement. By tracking the cross-bank movement of the center of each dye patch, *Houghton* [2002] estimated an on-bank diapycnal velocity of about 1.6 cm/s on the southern flank and 3.1 cm/s on the northeastern flank. These values are surprisingly close to the near-bottom, cross-bank Lagrangian residual velocities derived from both 2-D and 3-D model results of particle tracking for cases with idealized stratification [*Chen and Beardsley*, 1998; *Chen et al.*, 2003a]. This agreement should be viewed with caution, however, because they may accidentally match for different physical reasons.

[6] Most previous model studies have been "process-oriented" due in part to the lack of direct tracer measurements [*Loder and Wright*, 1985; *Chen*, 1992; *Naimie et al.*, 1994; *Chen et al.*, 1995, 2003a; *Naimie*, 1996, *Franks and Chen*, 1996, 2001; *Loder et al.*, 1997; *Chen and Beardsley*, 1998; *Pringle and Franks*, 2001; *Dale et al.*, 2003]. Recently, two studies have been published that compare model simulations with the dye experiment of *Houghton* [2002] conducted on the southern flank of GB during 22–26 May 1999. *Dong et al.* [2004] applied an idealized 2-D finite difference model to study diapycnal flow of a passive tracer released near the bottom just off-bank of the tidal mixing front on the southern flank of GB. While this simple model showed a qualitatively consistent on-bank diapycnal Lagrangian current (similar to that reported in an earlier 2-D Lagrangian experiment by *Chen and Beardsley* [1998]) and illustrated the sensitivity of the cross-frontal motion to the location and timing of the initial tracer injection, the 2-D model was unable to reproduce the observed trajectory of the dye patch, which is clearly influenced by an energetic 3-D mesoscale field of frontal structure and circulation. In the second study, *Aretxabaleta et al.* [2005] compared the trajectories of model drifters with the path of the center of the dye patch (as determined using the field measurements). By assimilating the shipboard ADCP velocity into a 3-D finite element model (QUODDY), they obtained a distinct on-bank movement of particles, generally similar to the observed trajectory of the center of the dye patch. A similar model drifter and dye comparison study was reported by *Proehl et al.* [2005] for an independent tracer release field experiment conducted on the northern flank in early June 1999 by Ledwell and coworkers. This study also showed reasonable agreement between the trajectories of model ensemble drifters and the observed center of the dye patch.

[7] These three recent model-dye studies provide insight into cross-frontal transport on GB but leave some key questions unanswered. What are the dominant processes that control the movement and horizontal/vertical dispersion of dye in the southern flank tidal frontal zone? What are the horizontal and vertical grid resolutions needed to obtain a convergent solution for both currents and dye dispersion? Is assimilation of in situ hydrographic and/or current data required to reproduce the observed dye patch structure and its temporal evolution?

[8] As part of the GLOBEC/GB Phase IV program, we applied the unstructured-grid Finite-Volume Coastal Ocean Model (FVCOM) to the GoM/GB region [*Chen et al.*, 2003b, 2004, Chen et al., Tidal dynamics in the Gulf of

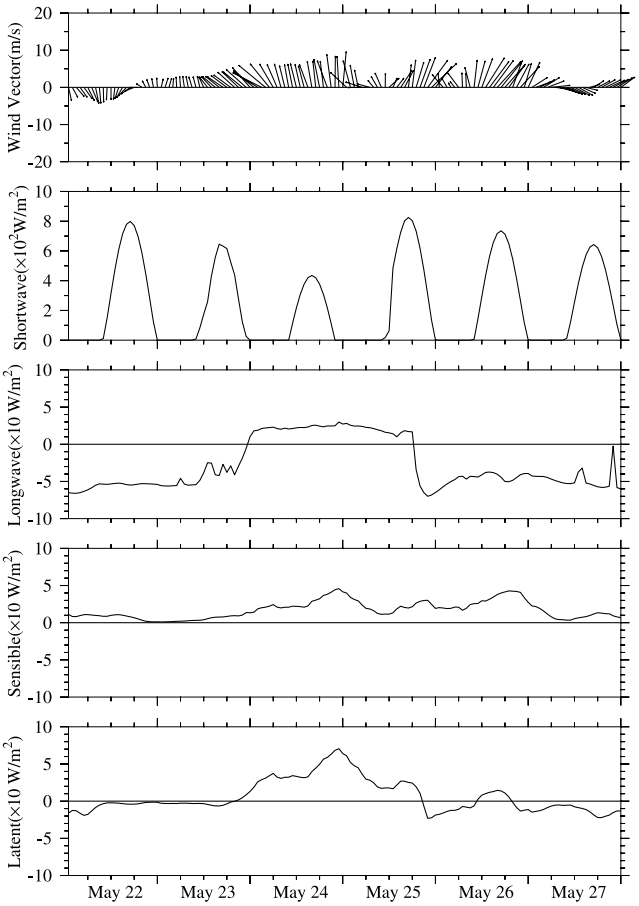

Figure 2. Time series of MM5-computed surface wind velocity vector, the short- and long-wave radiative heat fluxes, and sensible and latent heat fluxes at the center of the dye study area shown in Figure 1. The MM5 model results were validated with field measurements taken on NOAA buoys and US GLOBEC heat flux measurements [*Chen et al.*, 2005].

Maine and New England Shelf: An application of FVCOM, submitted to *Journal of Geophysical Research*, 2006, hereinafter referred to as Chen et al., submitted manuscript, 2006, 2007]. FVCOM is designed to combine the geometric flexibility found in finite element models and the computational efficiencies found in finite difference models. The discrete approach based on the flux calculation of the integral form of the governing equations guarantees mass conservation in individual control volumes for tracer equations, which is critical for accurate tracer-tracking studies in the coastal ocean. With various configurations of the unstructured-grid on GB, we have used FVCOM to simulate Houghton's 22–26 May 1999 southern flank dye experiment. These numerical experiments were directed at better understanding the processes controlling the dye patch movement and evolution while making detailed comparison between the model dye and observed dye behavior and identifying critical needs for future GB modeling.

[9] Results of these experiments are summarized in this paper following a discussion on critical issues on both modeling and the field measurements made to track the dye. The remaining sections of this paper are organized as follows. In section 2, the configuration of FVCOM and design of the numerical experiments are given, with a brief description of the dye-tracking experiment and meteorological conditions. In section 3, the results of the simulation and assimilation experiments are presented, with a direct comparison with the location of the dye center and shape observed in the Scanfish transects. In section 4, the dye cross-isobath dispersion is estimated. In section 5, the dynamics driving the trajectory of the dye's center is studied, with an evaluation of the relative importance of the ensemble dye velocity and vertical shear of the local velocity. In section 6, conclusions are summarized and some critical issues on model studies of cross-frontal water exchange on GB are discussed.

2. Numerical Experiment Design

[10] Three dye injections were made during the 1999 GB dye field study by Houghton and coworkers: two at the off-bank edge of the tidal mixing front on the southern flank and one at the edge of the northeastern flank [*Houghton*, 2002]. The first injection was made at a depth of 2.1 m above the bottom (the injection depth was 61.5 m and water depth was 63.6 m) at 67° 23.17′ W, 41° 4.58′ N on 22 May. The second injection was made at a depth of 6 m above the bottom at 67° 25.29′ W, 41° 4.50′ N on 27 May. The locations of these two injections were very close and the water depth at both locations the same. The third injection was made at a depth of 6 m above the bottom at 66° 54.81′ W, 42° 6.21′ N on 2 June. We selected the first injection for the model-dye comparison experiments, because it showed a significant on-bank movement of the dye patch (Figure 1).

[11] The first dye injection began at 15:55 GMT on 22 May during slack cross-bank tidal flow and a weakly southwest wind of <5 m/s (Figures 1 and 2). The injection lasted for 40 m, during which the water temperature (T) and salinity (S) in the injection area were 6.87°C–6.12°C and 32.38, respectively. The dye survey was carried out by towing a Scanfish (carrying a Chelsea Aquatracka III fluorometer and a SBE 19 SEACAT Profiler) through the water column at a ship speed of 6 knots. The center of the dye concentration at seven selected reference times (shown in Figure 1) was determined using at least six cross-bank Scanfish transects with an empirical adjustment of the T, S, and fluorescence fields to the selected reference time. The groups of transects used to define each dye patch covered a time interval of about 3–7 h under different tidal current conditions (Figure 3). A significant frontal perturbation propagated across the study area after 22:33 PM on 24 May, which is evident in vertically averaged T and S fields (Figure 4). Winds were generally northward during 23–26 May. Since the cross-bank scale of this perturbation was about 20 km (about twice as large as the local tidal excursion), we hypothesized that it was a result of a meander of the tidal mixing front due to a local interaction of tidal- and wind-driven flows.

[12] The model-dye comparison experiments were conducted using FVCOM [*Chen et al.*, 2003b, 2004, Chen et al., submitted manuscript, 2006, 2007]. There are two key

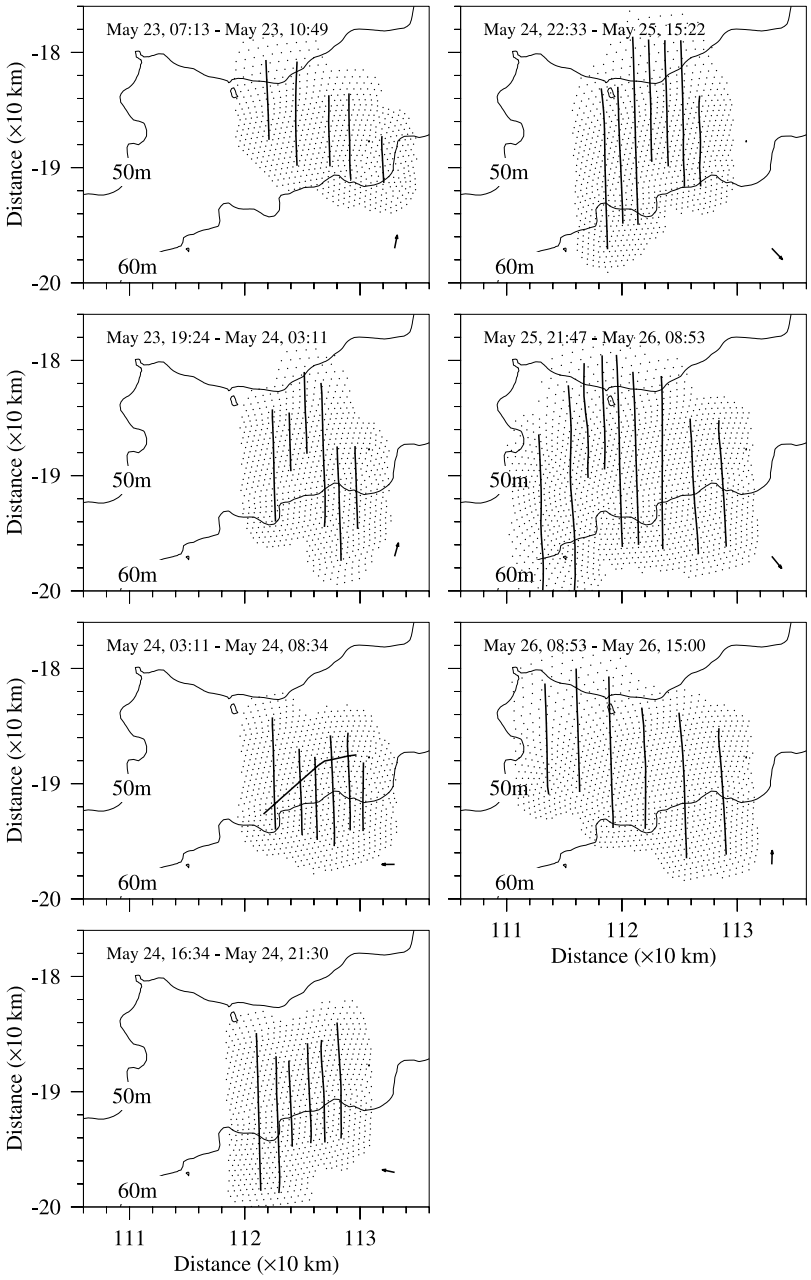

Figure 3. The patch areas used to determine the center of the dye concentration during the Scanfish surveys. The solid lines are Scanfish tracks. The dots are the node points of the unstructured grid included in the one-way nested local domain model experiment. In the lower right corner of each plot is the mean near-surface tidal current vector predicted by the FVCOM-based tidal forecast system during the tracks. In the upper part of each plot is the duration of that patch survey.

reasons why we chose FVCOM for this study. First, it is simple to re-configure the unstructured triangular grid mesh used in FVCOM to increase the horizontal resolution in a given sub-area of the model domain (e.g., the dye study area) needed to approach a convergence solution. Second, FVCOM was designed to ensure mass conservation in both the individual control volume and the entire computational domain. In such a mass-conserving model, a scalar tracer can be distorted by the flow but the total amount of tracer remains constant. If a model does not conserve mass locally, numerical damping can produce an unrealistic tracer concentration, which makes it difficult to estimate the impact of physical processes on the movement and distribution of the tracer. The second-order accurate flux calculation used in FVCOM avoids the loss of tracer due to numerical damping.

[13] The FVCOM domain used in this study covered the GOM/GB region and was enclosed by an open boundary running from the New Jersey shelf to the Nova Scotia shelf (Figure 5). The horizontal grid resolution varied

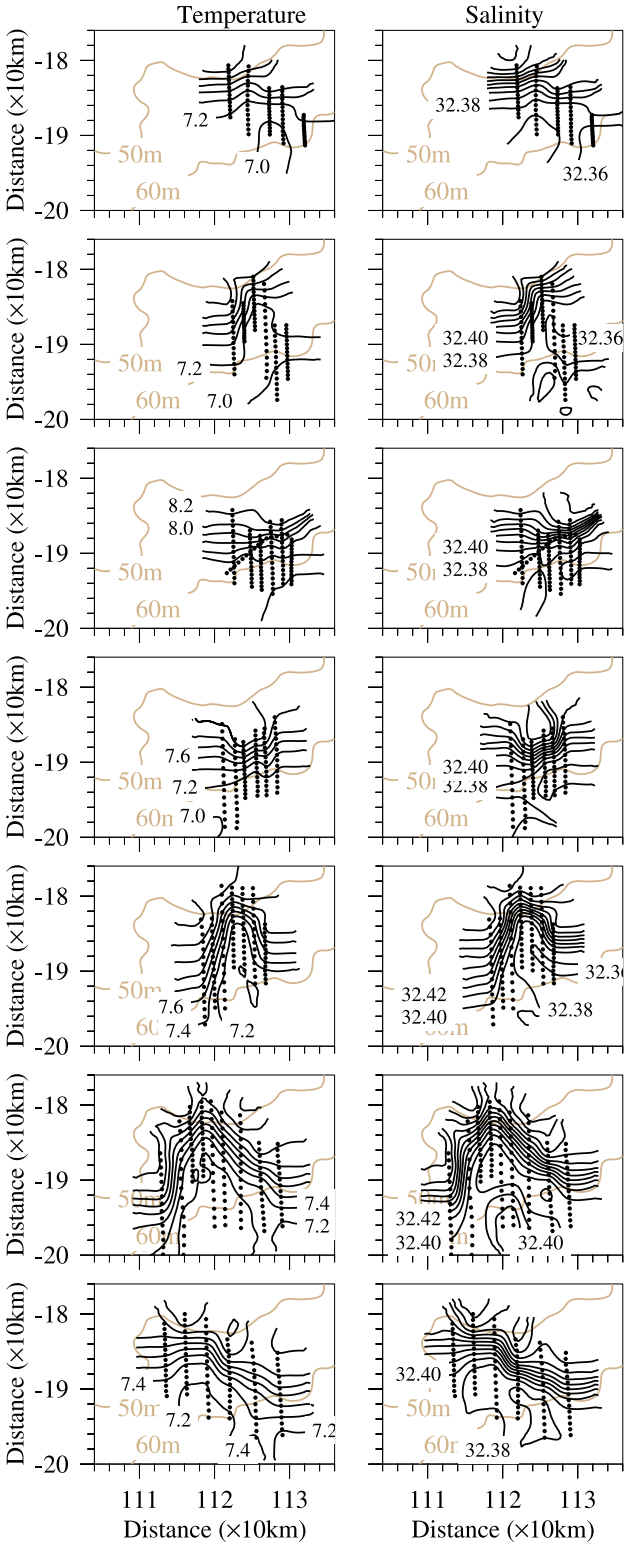

Figure 4. Vertically averaged temperature and salinity fields constructed using the hydrographic data collected during the seven patch surveys shown in Figure 3.

from ~1.0 km on the northern flank of GB to ~2–4 km over the southern flank of GB, Browns Bank, and inner shelf coastal regions, and then to ~10 km near the open boundary. FVCOM used the σ-coordinate system in the vertical, with 31 evenly spaced σ-levels, which corresponds to a vertical resolution of 2 m on the 60-m isobath over GB. To resolve the meso-scale variability of the tidal mixing front on GB and to examine the influence of local bathymetry on the movement and distribution of a dye patch, FVCOM was configured with regional and local computational domains. The regional domain was the same as that shown in Figure 5, except in the rectangular area in Figure 5 (in which the dye measurements were made) where four different horizontal resolutions were tested: 4 km, 2 km, 0.5 km, and 0.25 km (Figure 6). The local domain surrounded the area of the dye measurements taken from 23 May through 26 May. This domain was selected to include the seven dye patch areas mapped during the Scanfish surveys (Figure 3). The areas of these local domains changed with time and had different boundaries.

[14] We note here that one critical issue in these model-dye comparisons is the lack of exact initial conditions for T and S. The in situ dye-tracking measurements were made in a region with a spatial scale of about 10–20 km over a timescale of a few days. Although a few Scanfish transects were made before the dye was injected, these transects were too close in space to provide good spatial coverage that could be used to set up the initial T and S fields for the model run. The Scanfish CTD surveys showed significant small- and meso-scale variability in both T and S, which were not resolved in either monthly climatologies or the monthly GLOBEC/GB broad-scale hydrographic surveys taken in 1999. Merging the Scanfish CTD data into the regional climatology fields causes big T and S gradients around the boundary of these data sets, which can produce unrealistic buoyancy-driven currents. For this reason, we conducted both "simulation" and "assimilation" experiments with regional and local domains.

[15] The simulation experiments were designed to examine the model performance for a given set of initial conditions based on climatology and survey data and different model grid resolution. In these experiments, the model was driven using real-time tidal forcing applied on the open boundary, and surface forcing (wind stress and heat flux) and short-wave radiation in the upper water column estimated using the regional GOM-MM5 meso-scale meteorological model and satellite data [*Chen et al.*, 2005]. The model was initialized with the field of tidal currents and elevation at 00:00 AM on 1 April predicted using the tidal forecast FVCOM model and spun up for 15 days. At 00:00 16 April, T and S fields based on an April hydrographic climatology (The data sources used to build this climatology field are listed on our website: http://fvcom.smast.umassd.edu research_projects/GB/climatologic_mean.html) for the entire domain combined with the April 1999 GLOBEC/GB broad-scale survey data on GB were inserted into the model and the model then run for an additional 15 days until 30 April. Meteorological forcing was added at 00:00 AM 1 May and the numerical integration continued to 00:00 AM 27 May. Four experiments were conducted, with horizontal resolutions of 4, 2, 0.5,

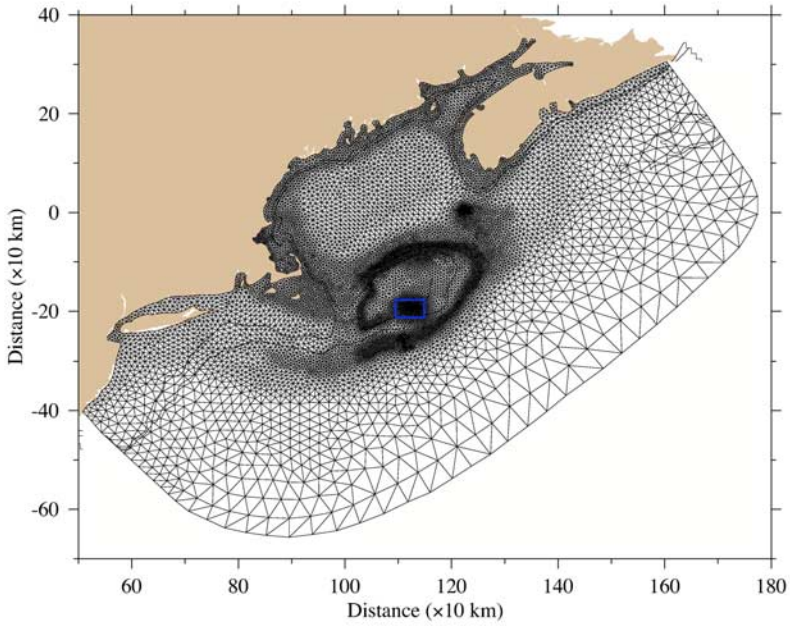

Figure 5. Unstructured triangular grid of the Gulf of Maine/Georges Bank FVCOM. In this case, the horizontal resolution in the dye study region is 0.5 km.

and 0.25 km in the dye study area, respectively. None of these experiments included the Scanfish survey data. The external mode time step was 120 s for the 4- and 2-km resolution cases, 60 s for the 0.5-km case, and 30 s for the 0.25-km case. The ratio of external mode time step to internal mode time step was 10 for these four cases.

[16] The assimilation experiments were designed to examine the impact of observed meso-scale variability of T and S within the tidal frontal zone and model grid resolution on the movement and distribution of a dye patch. In these experiments, the T and S data from the seven Scanfish dye surveys (shown in Figure 3) were interpolated objectively in space and time to individual model nodes, and assimilated into the local domain model runs. In detail, a restart file with the output from the simulation run was built on 22 May before the start of the dye injection. The local domain model first ran for the domain shown in Figure 3a with an initial field specified using the restart file output from the simulation run on 22 May. The observed T and S at nodes were nudged into the model at the mid-time of the first survey with a 3-h weight function window. The assimilation continued until the end of the first survey, and the results at the last time step saved into a file. The model was then re-started for the domain shown in Figure 3b with an initial field specified using a combination of the outputs from the first local domain assimilation and regional domain simulation runs. This initial field was checked carefully to ensure that no discontinuous features existed in the T, S, and current fields. The same nudging data assimilation procedure used for the first local domain run was then repeated for each of the successive Scanfish survey local domain runs. All assimilation experiments were made using one-way nesting, with no feedback to the regional domain model. (We also tried to conduct the assimilation experiments simultaneously within the regional domain. Because there was a big jump between observed and simulated water temperatures at the outer edge of each patch area, the two-way nesting model run after assimilation showed a large gradient in T, S, and thus density at the edge of the local domain. Sensitivity experiments were conducted by increasing the search radius of nudging in the outward direction; these showed little influence on the model results around the center of the dye patch for a few h after each assimilation event. For this reason, since our focus is on the dye patch behavior, we chose to use one-way nesting.)

[17] The nudging data assimilation method used in this study is briefly described here. Let $\alpha(x, y, z, t)$ be a variable selected to be assimilated and $F(\alpha, x, y, z, t)$ presents the sum of all the terms in the governing equation for α except the local temporal change term, then the governing equation for α with nudging assimilation is given as

$$\frac{\partial \alpha}{\partial t} = F(\alpha, x, y, z, t) + G_\alpha \cdot \gamma \cdot W \cdot (\alpha_o - \hat{\alpha}) \tag{1}$$

where α_o is the observed value, $\hat{\alpha}$ is the model-predicted value, γ is the data quality factor with a range from 0 to 1, G_α is a nudging factor that keeps the nudging term scaled by the slowest physical adjustment process, and W is the weight function defined as

$$W = \begin{cases} 1, & |t - t_o| \le 0.5T_w \\ \frac{2(T_w - |t - t_o|)}{T_w}, & 0.5T_w < |t - t_o| \le T_w \\ 0, & |t - t_o| > T_w \end{cases} \tag{2}$$

where T_w is the assimilation time window, t is the model integration time, and t_o is the time at which the observed data is input. In our experiments, $G_\alpha = 0.0076$, $\gamma = 1$ and $T_w = 3$ h.

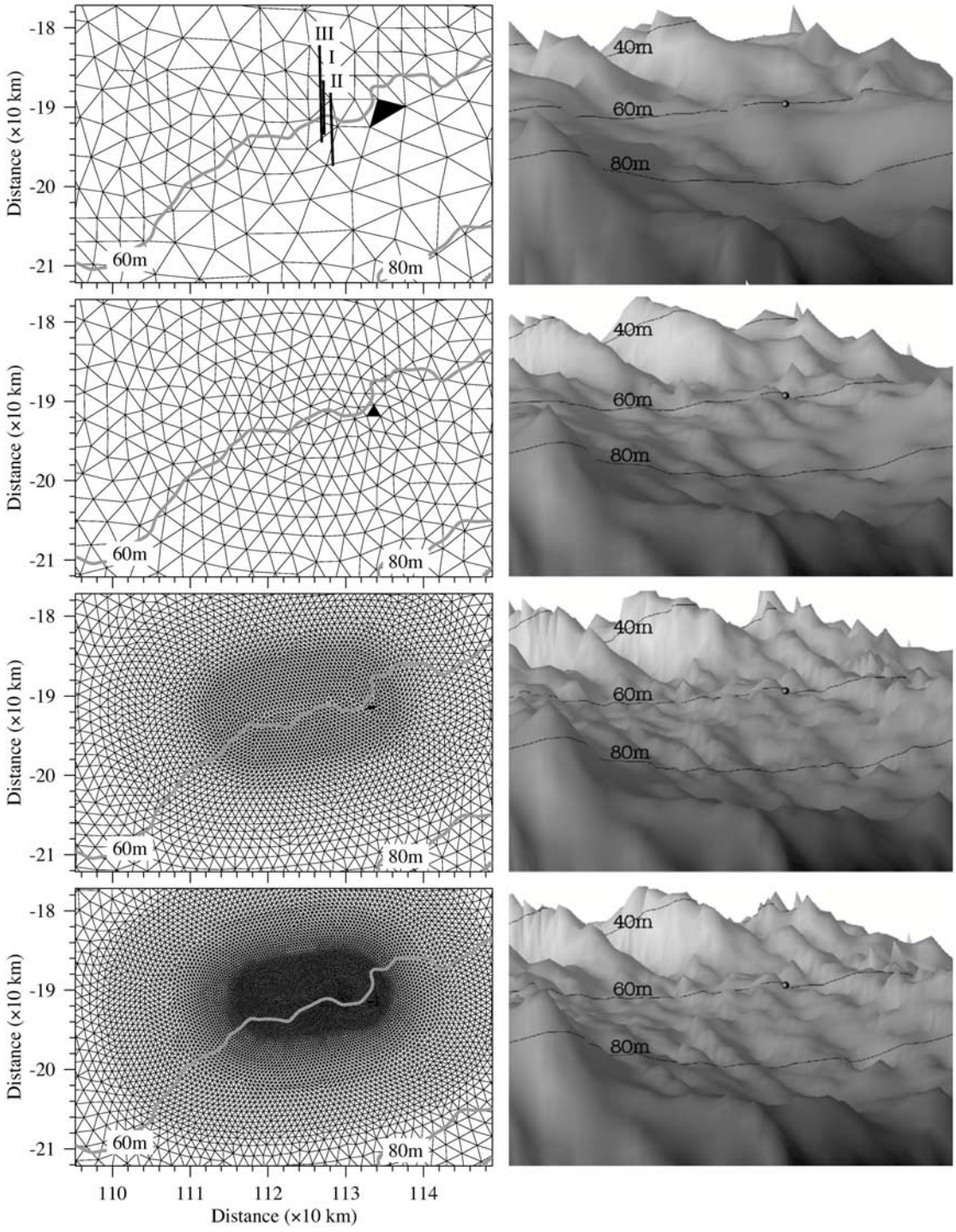

Figure 6. Unstructured triangular grids (left) and 3-D bathymetries in the dye study region for the cases with horizontal resolution of 4 km, 2 km, 0.5 km, and 0.25 km. The filled triangular area (in the left panels) show the grid cells where the dye was injected, and the ball (in the right panels) indicates the dye injection location. In the upper left figure, I, II, and III are the three Scanfish sections shown in Figures 9–11.

[18] The model dye was tracked by a tracer equation defined as

$$\frac{\partial DC}{\partial t}+\frac{\partial DuC}{\partial x}+\frac{\partial DvC}{\partial y}+\frac{\partial \omega C}{\partial \sigma}-\frac{1}{D}\frac{\partial}{\partial \sigma}\left(K_h\frac{\partial C}{\partial \sigma}\right)-DF_c = DC_o(x,y,\sigma,t) \quad (3)$$

where C is the model dye concentration, D is the total water depth, u, v, and ω are the x, y and σ components of water velocity, K_h is the vertical thermal diffusion coefficient, F_c is the horizontal diffusion term, and C_o is the concentration injected from a source point given as

$$C_o(x,y,\sigma,t)=\begin{cases}1 & t_s\le t\le t_e;\sigma_{28th}\le\sigma\le\sigma_{30th};x=\{x_i\};y=\{y_i\};i=1,N\\ 0 & \text{otherwise}\end{cases} \quad (4)$$

where t_s and t_e are the start and end times of the model dye injection, σ_{28th} and σ_{30th} refer to the 28th and 30th σ-levels, i is the node ID, and N is the total node numbers where the dye is injected. K_h is calculated using the modified Mellor and Yamada (MY) level 2.5 turbulence scheme implemented in FVCOM [*Mellor and Yamada*, 1982; *Chen et al.*, 2004] and the horizontal diffusivity in F_c is calculated using the Smagorinsky eddy parameterization method [*Smagorinsky*, 1963].

[19] The model dye was injected within the 28th–29th σ-layers (about 2 m above the bottom) starting at 15:55 PM 22 May and lasting 40 m similar to the field experiment (Figure 6). For the cases with horizontal resolution of 4 and 2 km, the model dye was injected at the three nodes of a triangular cell. In these two cases, the center of the triangle was the location where the observed dye was injected. For the case with a horizontal resolution of 0.5 km, the model dye was injected at eight nodes of six triangles, chosen so that the area bounded by these triangles has about the same shape as the original patch injected during the dye survey. For the case with a horizontal resolution of 0.25 km, the model dye was injected at ten nodes of eight triangles.

[20] The model-predicted distributions of dye concentration are compared here directly with the in situ dye concentration measurements from the Scanfish surveys. The model data used for these comparisons were sampled along the same track as the Scanfish in both time and space. This method avoids any bias caused by an empirical spatial/temporal adjustment of the dye measurements to estimate the "center" of the dye patch at a specific time since the dye survey was made over a period of several hours within an energetic bottom boundary layer within the tidal mixing front.

[21] We also made comparisons between trajectories of the centers of the model dye concentration and fluid particles. The particle tracking experiments were carried out using the fully 3-D Lagrangian tracking program for strong nonlinear flow systems implemented in FVCOM. The classical four-stage explicit Runge-Kutta algorithm was used for the Lagrangian time integration. A detailed description of this algorithm was given in the FVCOM user manual [*Chen et al.*, 2004].

3. Simulation and Assimilation Results

[22] Both advective movement and diffusion of the model dye were sensitive to the horizontal resolution used in the study region. The numerical solutions converged as the horizontal resolution was improved to 0.5 km. The model-dye comparison shown in this section is based on model results for the 0.5-km resolution case. A detailed discussion of the effects of horizontal resolution is given in section 4.

[23] The center of the model dye concentration is defined as

$$x_c(t)=\int\int_A \bar{C}hxdxdy/\int\int_A \bar{C}hdxdy;\ y_c(t) = \int\int_A \bar{C}hydxdy/\int\int_A \bar{C}hdxdy \quad (5)$$

where x_c (t) and y_c (t) are the x and y locations of the center of the dye concentration at time t, A is the horizontal area of the dye patch, $\bar{C}=\int_{-H}^{-H+h} C(x,y,z,t)dz$ is the vertically averaged dye concentration, $H = H$ (x, y) is the mean water depth, and $h = h$(x, y, t) is height measured from the bottom (Figure 7). The center of the model dye concentration on a Scanfish transect (S_c) is defined as

$$S_c=\int_L \bar{C}hldl/\int_L \bar{C}hdl \quad (6)$$

where l is the coordinate along the Scanfish track at the origin at the start time and L is the interval where the dye concentration is greater than 10^{-3} of the maximum concentration on the section. The centers of the model dye concentration computed from the simulation and assimilation experiments differed significantly. The first followed the tidal excursion ellipse with a mean movement paralleled to the 60-m isobath (Figure 8: upper-left), whereas the latter showed a significant cross-isobath, on-bank movement (Figure 8: upper-right). It was clear that the assimilation experiment resolved the on-bank movement of the dye concentration observed during the dye experiment, but the simulation experiment did not.

[24] Direct comparisons were made between the model-computed and observed dye structure and concentration on Scanfish transects. On a Scanfish transect taken from 8:33 to 9:08 GMT 23 May, about 16 h after dye injection, the dye patch was observed within the tidal frontal zone, which was about 5 km wide at the bottom and 45 m high in the water column (Figure 9: left panels). On the off-bank side of the dye patch, the water was weakly stratified in the upper 20 m in both temperature and salinity. Driven by the real-time wind stress and heat flux, the simulation experiment did produce a positive on-bank temperature gradient, but its intensity was much weaker than observed (Figure 9: middle panels). Since no salinity was input from the boundary and the surface precipitation/evaporation flux was zero, the simulated on-bank salinity gradient was opposite to observed. As a result, the model-computed dye patch on this transect extended throughout the entire water column. Although the width of the simulated model dye concentration was similar to the observed, the location of the dye's center drifted southward about 1.0 km. When the Scanfish hydrographic data was assimilated, the model produced cross-

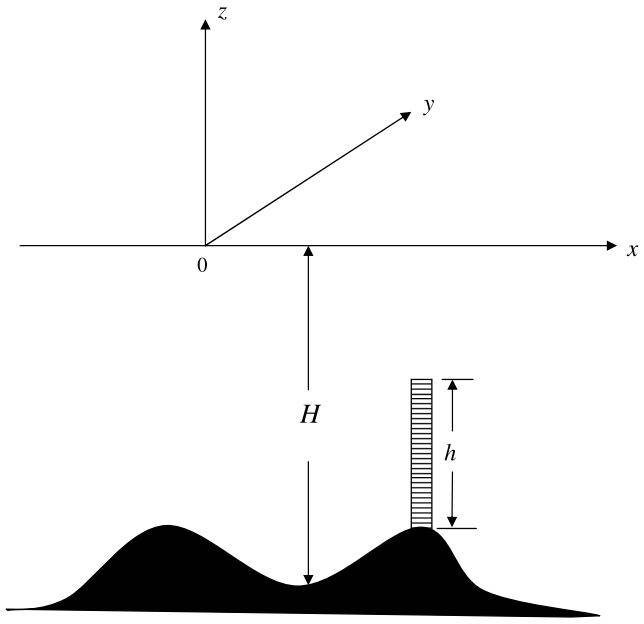

Figure 7. Schematic of the definition of the water depth and dye height in the Cartesian coordinate system.

isobath temperature and salinity distributions in good agreement with observation (Figure 9: right panels). The increased near-surface stratification suppressed the vertical mixing of the dye column. In this assimilation case, the model-computed location of the center of the dye patch was very close to the observation, even though its width was slightly greater.

[25] Similar results were obtained for the Scanfish transect taken from 21:09 to 22:07 GMT 23 May, about 29 h after dye injection. With temperature and salinity assimilation, the assimilation experiment reproduced more closely the shape (width and height) of the observed dye patch than that in the simulation experiment (Figure 10), in large part due to the failure to capture realistic vertical circulation in the simulation experiment. In both cases, the center of the model dye patch is displaced toward the south. On Scanfish survey transect taken from 17:22 to 18:00 GMT 24 May, about 49 h after dye injection, the in situ measurements showed that the upper part of the dye patch tilted off-bank in the vertical, which followed the tilted temperature contours (Figure 11). This structure was captured in the assimilation experiment but not in the simulation experiment.

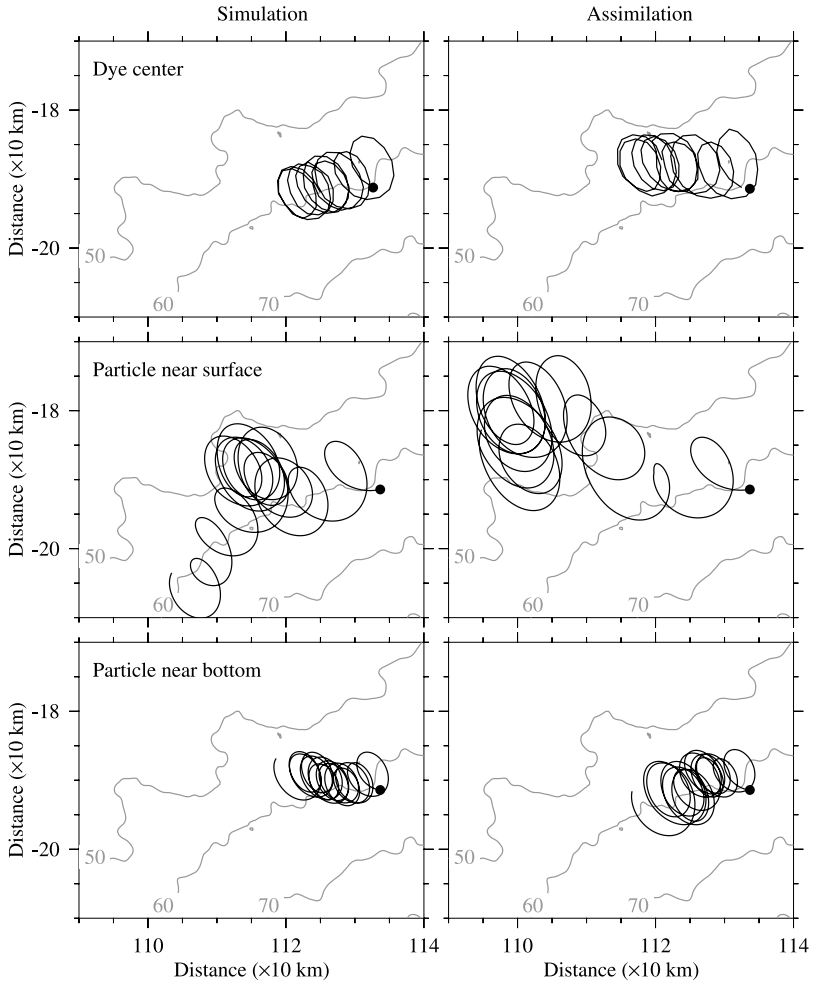

Figure 8. Trajectories of the dye center (upper), near-surface particle (middle) and near-bottom particle (bottom) for the simulation (left) and assimilation (right) cases. The large dot indicates the location where either dye was injected or the particle was released.

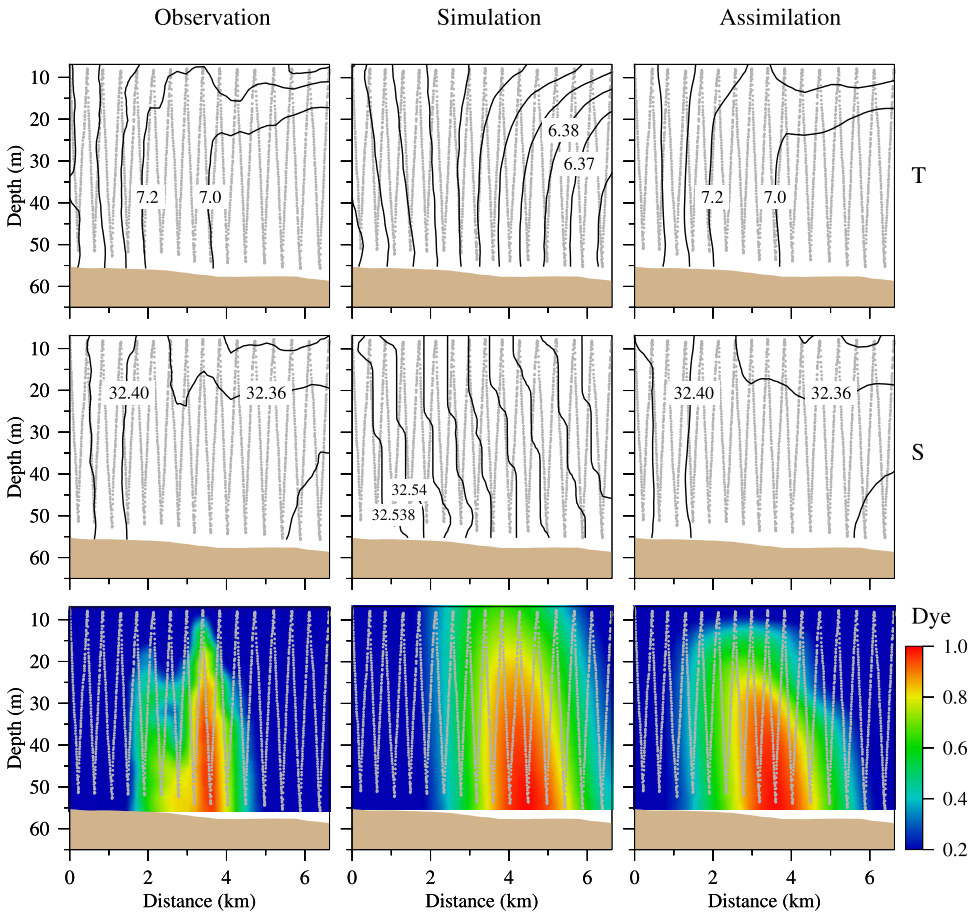

Figure 9. Distributions of observed (left), simulated (middle) and assimilated (right) water temperatures, salinities and dye concentrations on Scanfish section I. The light gray dotted line shows the Scanfish track.

[26] The location of the dye patch predicted in the assimilation experiment was not always in good agreement with the observations. A comparison was made between model-computed and observed locations of the center of the dye concentration on all the Scanfish transects taken between 2:44 GMT 23 May to 13:54 GMT 26 May during which a significant concentration of the dye was detected (Figure 12). The assimilation experiment showed reasonable tracking of the dye patch center detected on the transects, while the simulation experiment showed a southward drift of about 1.0–2.0 km in the location of the center of the dye patch, even though it showed a similar pattern of movement. The overall standard deviation, computed based on the difference between model-computed and observed locations of the centers of the dye patches on all available Scanfish transects, was 1.17 km for the assimilation case and 2.90 km for the simulation case.

[27] Displacements of the center of the model dye patch were coherent with the small-scale temporal variability of the tidal mixing front on the southern flank. In the simulation case, the model failed to resolve the small-scale variation of the tidal mixing front and thus the contours of water temperature were almost parallel to local isobaths. As a result, the model dye patch moved mainly along the local isobaths during which no significant tidally averaged on-bank movement was detected (Figure 13: left panel). In the assimilation case, the one-way nudging added the high-resolution Scanfish hydrographic data into the local computational domain to build realistic temperature and salinity fields within the tidal mixing frontal zone. The center of the model dye patch moved in direction almost parallel to contours of local temperature at the time it was "sampled", and a significant tidally averaged on-bank movement of the model dye patch occurred following the small-scale northward meander of the tidal mixing front (Figure 13: right panels). There was no evidence of a cross-frontal trajectory of the center of the model dye patch during the assimilation experiment. A large northward drift of the dye patch detected in the in situ dye measurements and assimilation experiment shown in Figures 1 and 8 was caused mainly by the periodic tidal variation. It was not surprising that the simulation experiment failed to capture the on-bank movement of the dye patch, because the initial temperature and salinity fields were specified using the monthly climatology hydrographic data with a horizontal resolution of 10 km and the surface meteorological forcing fields also had a resolution of 10 km.

[28] The Scanfish measurements showed that the mean water temperature of the dye patch increased with time during the May survey (Figure 14). It was about 6.9°C a few

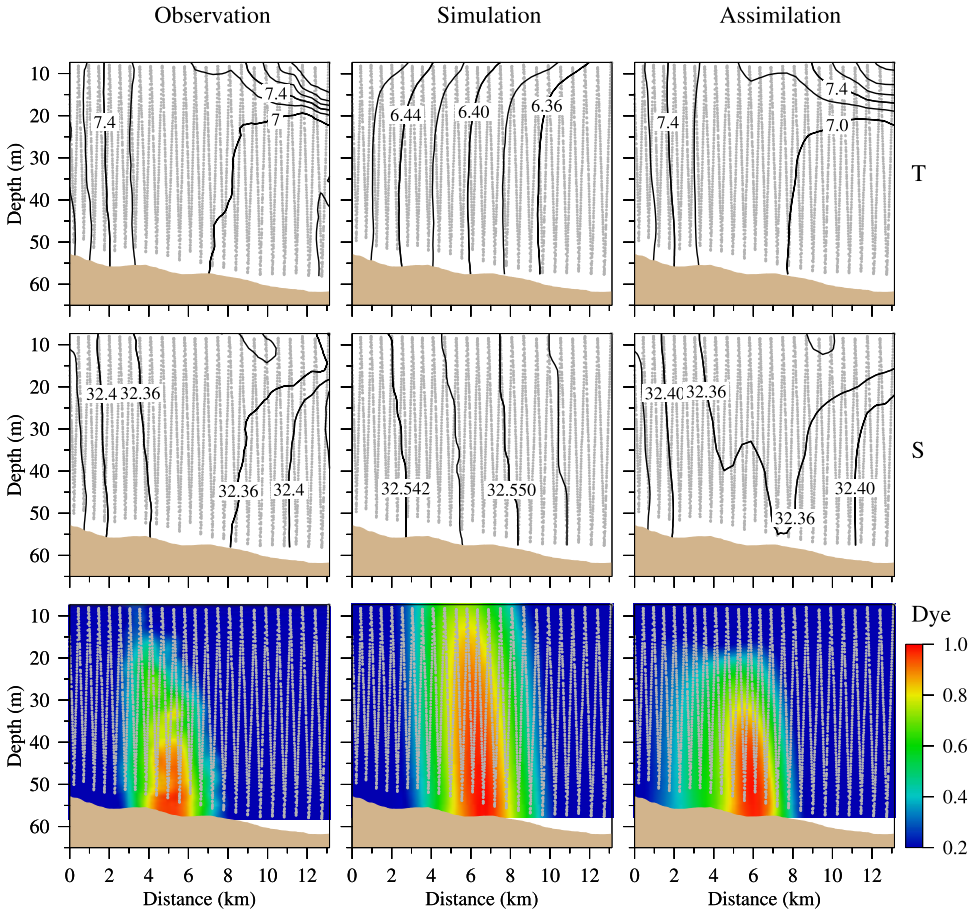

Figure 10. Distributions of observed (left), simulated (middle) and assimilated (right) water temperatures, salinities and dye concentrations on section II The light gray dotted line shows the Scanfish track.

hours after the dye injection and up to 7.3°C after 72 h (an increase of 0.4°C). This trend was captured reasonably well in the assimilation experiment after about 20 h of the nudging adjustment in temperature (and salinity) fields. The simulation experiment did show a warming tendency in the mean water temperature of the model dye patch. The background field of water temperature was about 0.55°C lower than the observed value at the beginning of the dye injection, however, the mean water temperature of the model dye patch increased only by 0.12°C after 100 h.

[29] Selecting the 7°C contour as a reference, *Houghton* [2002] calculated the cross-isobath velocity of the observed dye patch at four selected times during the Scanfish survey. He found that the on-bank velocity decreased as the distance from the 7°C contour increased. This suggested that the on-bank Lagrangian velocity decreased as the dye moved on-bank within the frontal zone. The model results indicate that the intensity and horizontal structure of the tidal mixing front varied significantly during the Scanfish survey. Since the orientation of the 7°C isotherm varied with the temporal variation of the front, the velocity via the distance from the 7°C contour found in the model was not always an indicator of the on-bank Lagrangian velocity within the frontal zone (Figure 13). We found that the cross-frontal Lagrangian velocity decreased quickly from 3 cm/s to 1 cm/s or less when the model dye center moved into the maximum temperature gradient area of the front about 1.5 days after the dye injection. This fact indicates a convergence zone near the bottom at the frontal zone, which is consistent with our previous 2-D and 3-D model experiment results [*Chen and Beardsley*, 1998; *Chen et al.*, 2003a].

4. Horizontal Resolution Via Horizontal Dispersion

[30] One of the critical issues in coastal modeling is the parameterization of horizontal diffusion. Like other popular coastal ocean models, the horizontal diffusion coefficient in FVCOM is either treated as a constant value or calculated using a Smagorinsky eddy parameterization method [*Smagorinsky*, 1963]. The Smagorinsky horizontal diffusivity for scalars is given as

$$A_h = \frac{0.5 C_H \Omega^{\zeta}}{P_r} \sqrt{\left(\frac{\partial u}{\partial x}\right)^2 + 0.5\left(\frac{\partial v}{\partial x} + \frac{\partial u}{\partial y}\right)^2 + \left(\frac{\partial v}{\partial y}\right)^2} \qquad (7)$$

where C_H is a constant parameter, Ω^{ζ} is the area of the individual tracer control element, and P_r is the Prandtl

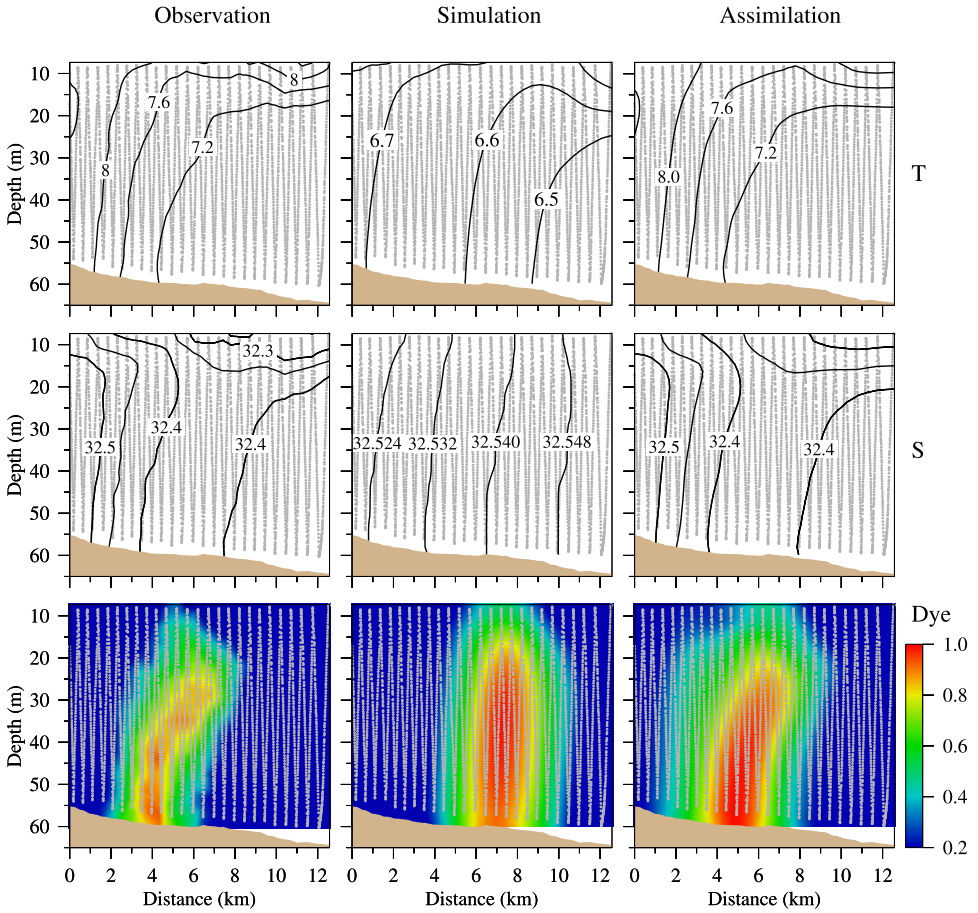

Figure 11. Distributions of observed (left), simulated (middle) and assimilated (right) water temperatures, salinities and dye concentrations on section III. The light gray dotted line shows the Scanfish track.

number. The value of A_h is proportional to the area of the individual tracer control element and the gradient of horizontal velocities: decreasing as the grid size and/or horizontal velocity gradient is reduced. In general, A_h is a function of time and space related to the horizontal current shear and bathymetry. On GB, for example, A_h is larger on the northern flank than on the southern flank due to the increased shear in the high current jet found along the northern flank [*Houghton*, 2002]. In some applications, however, this coefficient can be inferred through other data or empirical knowledge. Some structured-grid finite difference models are unstable without including horizontal diffusion. A_h in those models acts like a diffusive factor used to suppress numerical instability. FVCOM can run without horizontal diffusion, so that the horizontal diffusion terms in this model are considered physically meaningful. Because of the lack of direct measurements, we cannot answer the question whether or not this parameterization accurately represents the horizontal turbulent diffusion process on GB. The question raised here is for a given Smagorinksy parameterization, can FVCOM provide an accurate estimation of the cross-frontal diffusive flux?

[31] *Houghton* [2002] used the Fickian model to estimate the cross-frontal horizontal diffusion coefficient A_y from the in situ dye concentration measurements. In this model, A_y is defined as

$$A_y = 0.5\frac{\Delta V_y}{\Delta t} \tag{8}$$

where ΔV_y is the change of variance of the dye concentration during the time interval Δt. In Houghton's calculation, the lateral variation of the dye patch was estimated from the vertically integrated dye patch. V_y was equal to the minor axis of the lateral variance that was oriented approximately in the cross-frontal direction. The estimated values of V_y increased with time (Figure 15), which produced a time averaged A_y value of 18 $m^2/s \pm 4.5$ m^2/s [*Houghton*, 2002].

[32] We used here the same method to estimate V_y in the model dye experiments. For the model setup with $P_r = 1$ and $C_H = 0.4$, V_y estimated from the model-dye patch was sensitive to the horizontal resolution (ΔL) of the model grid (Figure 15), where ΔL denotes the length of the longest sideline of a triangular mesh. For the case with $\Delta L = 4.0$ km in the dye study area, the model significantly overestimated V_y. The model-estimated V_y increased rapidly with time, exceeding 120 km^2 after 4 days, about 12 times larger than the observed value. The model-predicted V_y converged

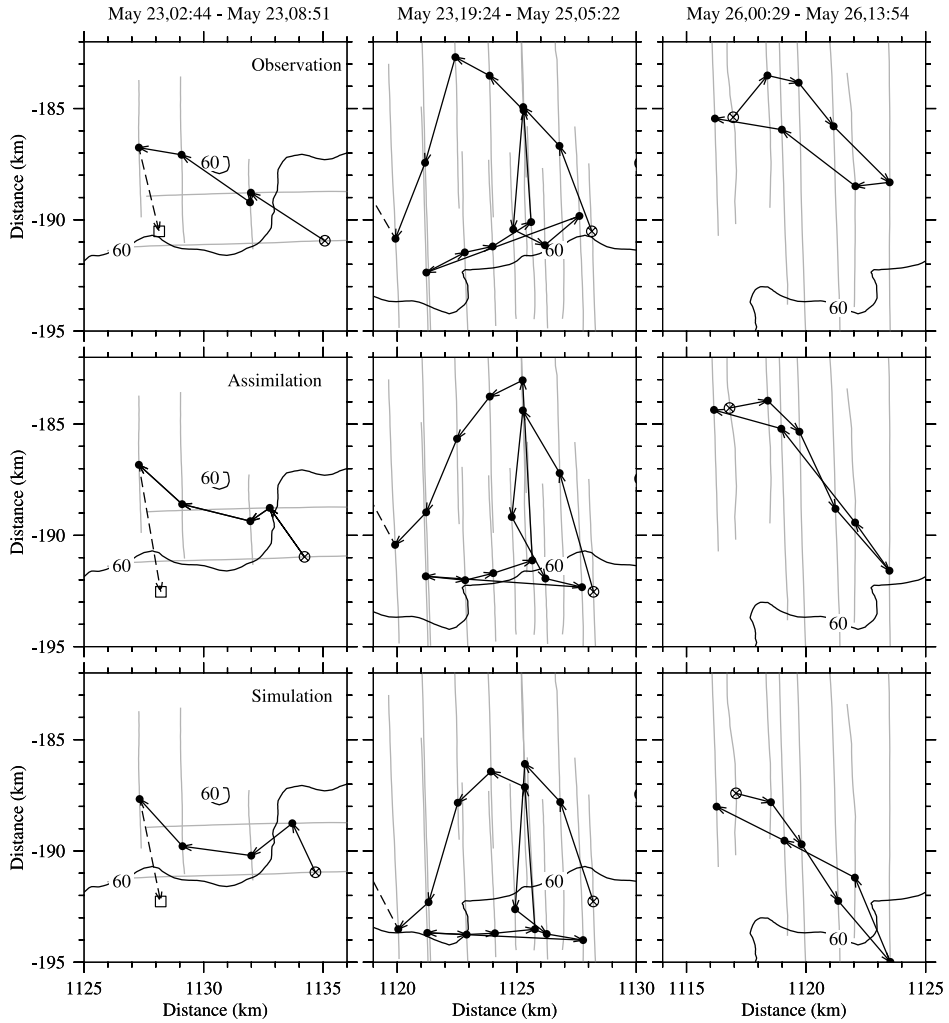

Figure 12. Locus of observed, assimilated and simulated dye center on Scanfish transects from 02:44 22 May to 08:51 23 May ; 19:24 23 May to 05:22 25 May; and 00:29 26 May to 13:54 26 May. The light gray dotted lines indicate the Scanfish transects.

rapidly toward the observed value with increasing horizontal resolution. With ΔL = 2.0 km, the model-calculated V_y after 4 days dropped to 50 km^2, 58% smaller than the value estimated in the case with ΔL = 4.0 km. With ΔL = 0.5 km, the time series of the model-predicted V_y agreed reasonably well with the observed. In these experiments, 0.5 km seemed to be the horizontal resolution required for a convergence solution of the cross-frontal variation of the dye patch, because the model-predicted V_y in the case with ΔL = 0.25 km remained almost identical to that estimated with ΔL = 0.5 km.

[33] In the area of the dye release and tracking, the model values of A_y decreased rapidly from O(100 m^2/s) for the case of ΔL = 4.0 km to O(10–20 m^2/s) for the case of ΔL = 0.5 km. A_y remained in O(10–20 m^2/s) as ΔL dropped to 0.25 km. This value is consistent with the convergence tendency found in V_y shown in Figure 15.

[34] If we believe the accuracy of the bathymetry data on GB used in the model, we need a high-resolution model with a horizontal grid size of ΔL = 0.5 km or less to resolve accurately the cross-isobath diffusive flux in the tidal mixing front on the southern flank. The bathymetry data used in this experiment were from a USGS digital bathymetric database with a horizontal resolution of 15 sec in latitude and longitude, which corresponded to roughly 0.4-km spacing. The flexibility of the unstructured triangular grid approach used in FVCOM makes it feasible to increase the horizontal resolution in the selected local region to obtain an accurate solution. It should be pointed out that the requirement for horizontal resolution to resolve lateral dispersion on GB reported here may not be directly applicable to other coastal systems, where different physical conditions and dynamics may create different scales of motion that in turn determine the spatial resolution required to resolve lateral dispersion.

5. Kinematics Driving the Movement of the Dye Patch

[35] The trajectory of the center of the model dye patch differed from trajectories of particles released near the bottom and surface (Figure 8). In the simulation experiment, a particle released near the surface showed a large oscillating trajectory, with a tidally filtered path toward the south-

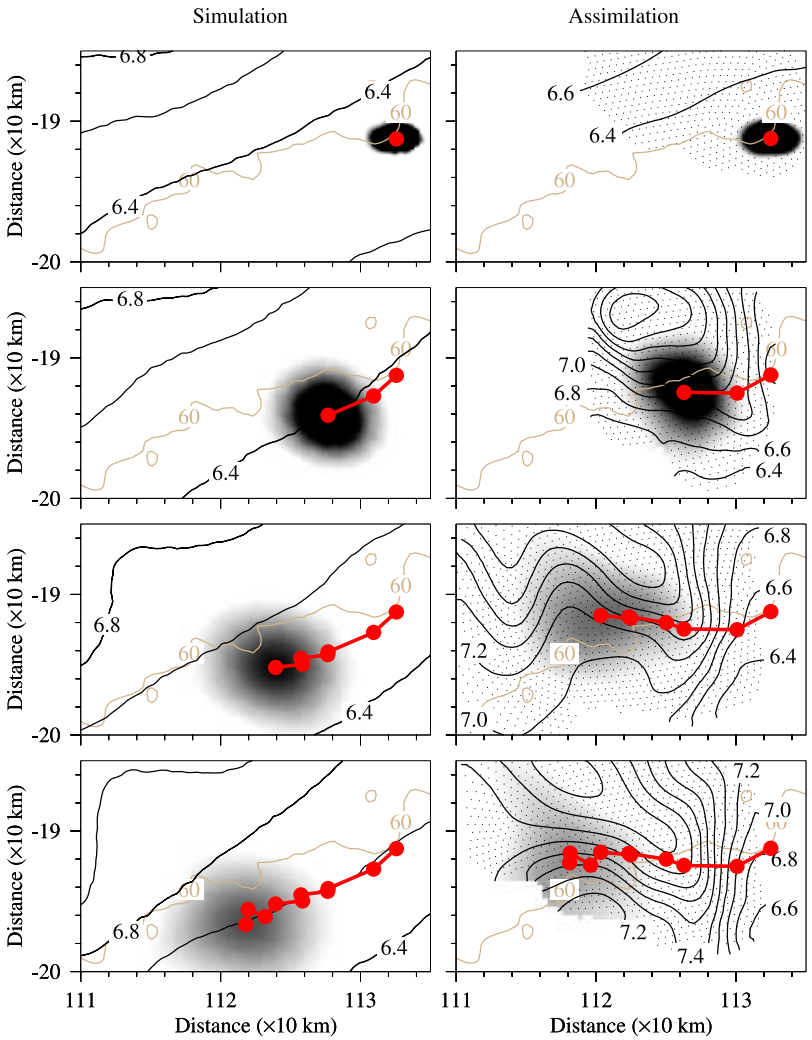

Figure 13. The distributions of the simulated (left) and assimilated (right) dye concentrations at 17:00 GMT 22 May (top row); 17:50 GMT 23 May (second row); 19:31 GMT 25 May (third row) and 8:47 GMT 27 May (bottom row). Light gray lines: bathymetric contours; solid lines: water temperature contours; and gray scale patch: the dye concentration. The large dots indicate the movement of the dye center in time. The temperature contours and dye patch correspond to the last location of the dye patch in each plot.

west along the 60-m isobath in the first two tidal cycles, then northward for about 10 km in the successive few tidal cycles, before returning to the south and then moving along the 60-m isobath again. A particle released near the bottom exhibited a tidal elliptical path with a tidally filtered on-bank motion with at a speed of about 1.0–2.0 cm/s. Unlike either near-surface or near-bottom particles, the center of the model-dye patch moved in a tidal elliptical path with a subtidal motion parallel to the local 60-m isobath.

[36] In the assimilation experiment, the near-surface particle moved quickly onto the crest of the bank and entered into a region shallower than 50 m, while the tidally filtered trajectory of the near-bottom particle was mainly parallel to the 60-m isobath. In this case, the tidally filtered path of the center of the dye patch showed a significant on-bank, cross-isobath movement, which differed from both near-surface and near-bottom particles. A large difference in the near-surface particle tracks found in the simulation and assimilation cases is due to stratification. In the assimilation experiment, the thermocline and halocline were established at a depth of about 5–10 m from the surface using nudging. As a result of the thin mixed layer, the wind-driven current in this case was much stronger than that found in the simulation case. For this reason, given the same wind conditions, near-surface particles released in the assimilation experiment drifted more quickly onto the bank than those released in the simulation experiment.

[37] The difference between particle and tracer trajectories raises a fundamental question about the physical mechanism(s) that govern the movement of the dye patch on GB. In the Cartesian coordinate system, equation (3) can be simplified as

$$\frac{\partial C}{\partial t}+\frac{\partial uC}{\partial x}+\frac{\partial vC}{\partial y}+\frac{\partial wC}{\partial z}-\frac{\partial}{\partial z}\left(K_h\frac{\partial C}{\partial z}\right)-F_c=C_o(x,y,z,t) \tag{9}$$

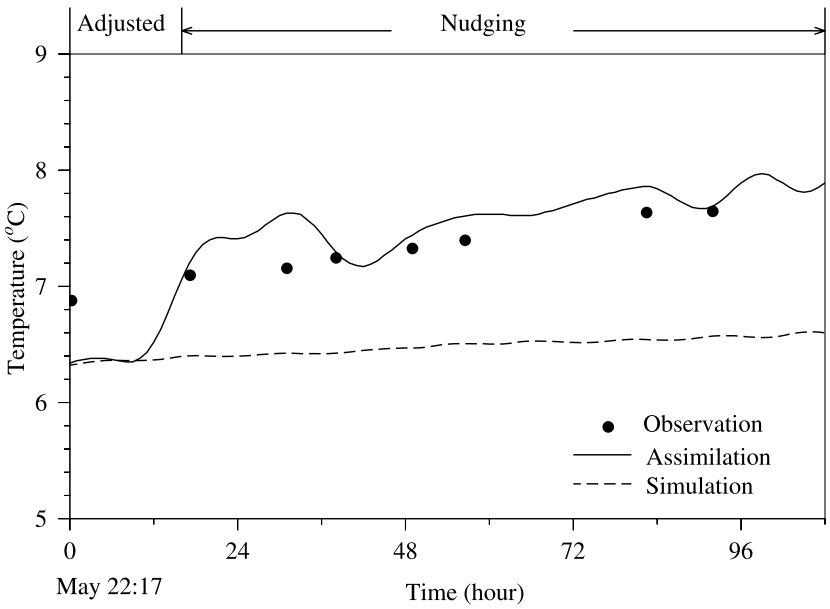

Figure 14. Time series of observed (dots), assimilated (solid line) and simulated (dashed line) vertically averaged water temperature at the dye center from 17 GMT 22 May to 5 GMT 27May. A 12-h low-passed filter is used to remove tidal variations in the assimilated and simulated water temperatures.

with

$$C = \bar{C} + C\prime,\ u = \bar{u} + u\prime,\ v = \bar{v} + v\prime \tag{10}$$

where $\overline{(\ )} = 1/h \int_{-H}^{-H+h} (\ )dz$, h is the height of the dye patch above the bottom, $\bar{C}$ is the vertically averaged concentration of the dye patch, $\bar{u}$ and $\bar{v}$ are the x and y components of the vertically averaged velocity of the dye patch, and C', u' and v' are the vertical perturbations relative to $\bar{C}$, $\bar{u}$ and $\bar{v}$. Substituting equation (10) into equation (9) and integrating it from -H to -H + h yields

$$\frac{\partial h\bar{C}}{\partial t} + \frac{\partial \bar{C}\bar{u}h}{\partial x} + \frac{\partial \bar{C}\bar{v}h}{\partial y} + \frac{\partial h\overline{c\prime u\prime}}{\partial x} + \frac{\partial h\overline{c\prime v\prime}}{\partial y} = h\bar{F}_c + h\bar{C}_o \tag{11}$$

Multiplying equation (11) by x and y, respectively, and then integrating them over the area of the dye patch, we can derive equations for the location of the center of the dye patch given as

$$\frac{dx_c(t)}{dt} = \frac{1}{\hat{C}}\left[\int\int_A \bar{C}(\bar{u}h)dxdy + \int\int_A h\overline{c\prime u\prime}dxdy + \int\int_A xh\bar{C}_o dxdy\right] \tag{12}$$

$$\frac{dy_c(t)}{dt} = \frac{1}{\hat{C}}\left[\int\int_A \bar{C}(\bar{v}h)dxdy + \int\int_A h\overline{c\prime v\prime}dxdy + \int\int_A yh\bar{C}_o dxdy\right] \tag{13}$$

where $\hat{C} = \int\int_A \bar{C}hdxdy$, and x_c (t) and y_c (t) are the x and y locations of the center of the dye patch at time t defined by equation (5). Equations (12) and (13) are derived with the assumption that the horizontal diffusive flux vanishes at the lateral edge of the dye patch.

[38] Equations (12) and (13) indicate that after the dye is released, the movement of the center of the dye patch is driven by the ensemble velocity defined as [($\bar{u}$h), ($\bar{v}h$] and the concentration flux related to the vertical shear of the horizontal velocity of the dye patch [($\overline{c\prime u\prime}$), ($\overline{c\prime v\prime}$)]. Which term is dominant in this dye study?

[39] We tracked the model dye patch using equations (12) and (13) and compared the time series of [x_c (t), y_c (t)] with that estimated for the model-computed dye patch directly

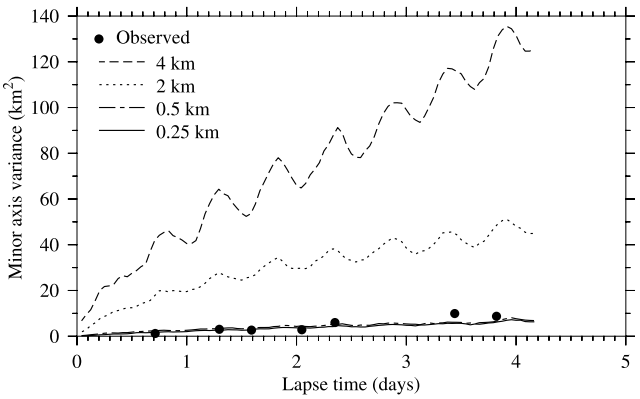

Figure 15. Time series of minor axis variance of dye patch versus lapsed time (from dye injection) for the numerical experiments with horizontal resolutions of 4 km, 2 km, 0.5 km and 0.25 km. The dots are the minor axis variance estimated from the in situ dye patch measurements.

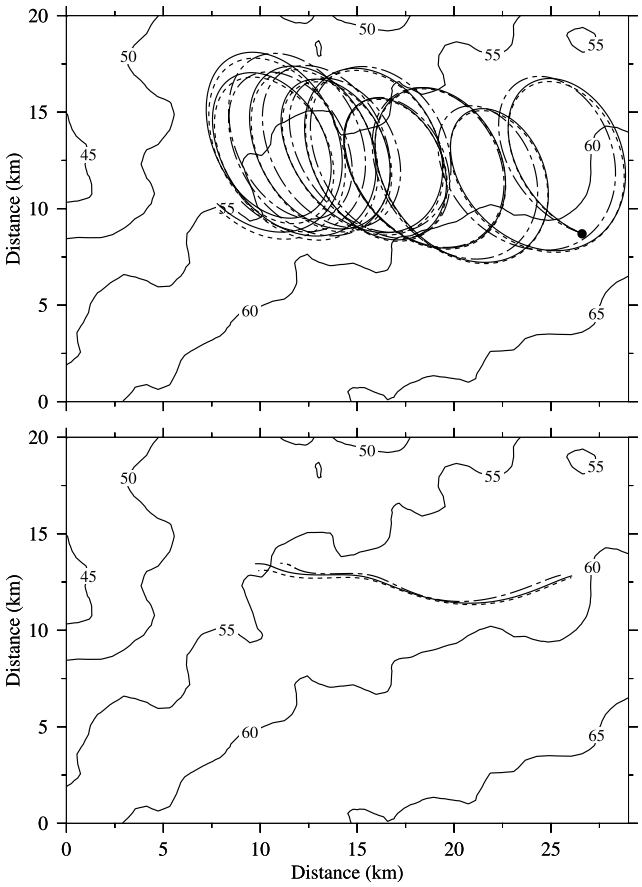

Figure 16. Trajectories of the dye center calculated with the model tracer equation (equation (3)) (solid line), equations (12)–(13) with inclusion of both ensemble and shear velocity terms (dashed line), and equations (12)–(13) without inclusion of the shear velocity term (dot-dashed line). Upper: trajectories constructed using the hourly output. Lower: the 40-h low-passed filtered trajectories for the three cases described above.

from equation (3). The results of these two methods are almost identical (Figure 16a). Comparison of the ensemble velocity and vertical shear terms in equations (12) and (13) showed that the ensemble velocity is the primary driving forcing for the dye patch but that the vertical shear is not negligible (Figure 16a). In this strongly tidal environment, the vertical shear term played a first-order correction of the dye path during the flood and ebb periods except at the tidal current transition time. Ignoring the vertical shear term caused a westward drift of the path of the center of the dye patch in both flood and ebb tidal periods. This drift varied with tidal cycles. Since the spatial variation of the amplitude of the tidal currents was very small in the local dye study region, the time-dependent structure of this westward drift was also related to local bathymetry and temporal variation in wind-forcing. A 40-h low-passed filter was used to generate the mean trajectory of the center of the model dye patch (Figure 16b). It is clear that ignoring the vertical shear term in equations (12) and (13) caused a slower movement of the center of the dye patch, with a 1.5-km shift in the location of the center of the dye patch. Although this shift is insignificant compared with the distance the dye moved over the entire simulation period, the first-order correction of the dye patch motion during the tidal cycle cannot be ignored if the study is aimed at the temporal variation of the dye patch movement on timescales less than a tidal period.

[40] The relative importance of the vertical shear term might vary under tidal current, wind and local bathymetry conditions. For the situation in which either vertical shear of the horizontal velocity or vertical gradient of the dye concentration equals zero, these terms vanish. This is one reason why these terms were very small during the tidal transition times on GB, when both tidal current and vertical shear were very weak. The significant contribution of the vertical shear term found in this dye study suggests that the dye patch was advected in a vertically inhomogeneous flow field. This is consistent with the differing trajectories of the near-surface and near-bottom particle tracks. In such an inhomogeneous flow field, one should be cautious when studying the movement of a dye patch using the Lagrangian particle approach.

6. Conclusions

[41] In this paper we use the unstructured-grid Finite-Volume Coastal Ocean Model (FVCOM) to hindcast the May 1999 dye study conducted by *Houghton* [2002]. We found that when nudging was used to assimilate the Scanfish temperature and salinity data, the FVCOM solution captures the structure and movement of the observed dye patch. Comparisons between model-computed and observed dye patch evolution for the simulation (without nudging) and assimilation cases suggest that the observed on-bank movement of the dye patch was caused by small-scale variability of the tidal mixing front orientation and intensity. The onset of vertical stratification tended to slow down an upward mixing of the dye column and trapped the dye within the bottom mixed layer. Within the tidal mixing front, the movement of the center of the dye patch was driven by the ensemble velocity integrated over the dye volume plus the dye concentration flux related to the vertical shear of the horizontal velocity in the dye patch. The trajectory of the center of the dye patch differed significantly from the trajectories of near-surface and near-bottom particles. A horizontal grid resolution of $\sim$500 m was required to resolve the dye patch spatial evolution and movement and provide a reasonable estimate of the cross-isobath diffusive flux.

[42] **Acknowledgments.** This research was supported by the U.S. GLOBEC Northwest Atlantic/Georges Bank Program NSF (OCE-0234545; OCE-0227679) and NOAA grants (NA-16OP2323) to Changsheng Chen and Qixchun Xu, NSF grant (OCE-0236270) to Robert Houghton, and the Smith Chair in Coastal Oceanography and NOAA grant (NA-17RJ1223) to R.C. Beardsley. The experiments were conducted using the Linux cluster computers of the Marine Ecosystem Dynamics Modeling Laboratory at the School of Marine Science and Technology, University of Massachusetts-Dartmouth, funded by the SMAST Fishery Program through NOAA grants DOC/NOAA/NA04NMF4720332 and DOC/NOAA/NA05NMF4721131. This paper is U.S. GLOBEC contribution number 537, 07-0602 in the SMAST Contribution Series, School of Marine Science and Technology, University of Massachusetts-Dartmouth and Lamont Doherty Earth Observatory contribution No 7061.

References

Aretxabaleta, A., J. Manning, F. E. Werner, K. Smith, B. O. Blanton, and D. R. Lynch (2005), Data assimilative hindcast on the southern flank of Georges Bank: Frontal circulation and implications, *Cont. Shelf Res.*, *25*, 849–874.

Chen, C. (1992), Variability of currents in Great South Channel and over Georges Bank: observation and modeling. Ph.D. Thesis, MIT/WHOI Joint Program, Technical Report WHOI-92-20, 283 pp.

Chen, C., and R. C. Beardsley (1998), Tidal mixing and cross-frontal particle exchange over a finite amplitude asymmetric bank: A model study with application to Georges Bank, *J. Mar. Res.*, *56*, 1165–1201.

Chen, C., and R. C. Beardsley (2002), Cross-frontal water exchange on Georges Bank: Some results from an U.S. GLOBEC/Georges Bank program model study, *J. Oceanogr.*, *58*, 403–420.

Chen, C., R. C. Beardsley, and R. Limeburner (1995), Variability of currents in late spring in the northern Great South Channel, *Cont. Shelf Res.*, *15*, 451–473.

Chen, C., Q. Xu, R. C. Beardsley, and P. J. S. Franks (2003a), Model study of the cross-frontal water exchange on Georges Bank: A 3D Lagrangian experiment, *J. Geophys. Res.*, *108*(C5), 3142, 10.1029/2000JC000390.

Chen, C., H. Liu, and R. C. Beardsley (2003b), An unstructured, finite-volume, three-dimensional, primitive equation ocean model: Application to coastal ocean and estuaries, *J. Atmos. Oceanic Tech.*, *20*, 159–186.

Chen, C., G. Cowles, and R. C. Beardsley (2004), An unstructured grid, finite-volume coastal ocean model: FVCOM User Manual. *SMAST/UMASSD Technical Report-04-0601*, 183 pp.

Chen, C., R. C. Beardsley, S. Hu, Q. Xu, and H. Lin (2005), Using MM5 to hindcast the ocean surface forcing fields over the Gulf of Maine and Georges Bank region, *J. Atmos. Oceanic Tech.*, *22*(2), 131–145.

Chen, C., H. Huang, R. C. Beardsley, H. Liu, Q. Xu, and G. Cowles (2007), A finite-volume numerical approach for coastal ocean studies: Comparisons with the finite-difference models, *J. Geophys. Res.*, *112*, C03018, doi:10.1029/2006JC003485.

Dale, A. C., D. S. Ullman, J. A. Barth, and D. Hebert (2003), The front on the northern flank of Georges Bank in spring: 1. Tidal and subtidal variability, *J. Geophys. Res.*, *108*(C11), 8009, doi:10.1029/2002JC001327.

Dong, C., R. Houghton, H. W. Ou, D. Chen, and T. Ezer (2004), Numerical study of the diapycnal flow through a tidal front with passive tracers, *J. Geophys. Res.*, *109*, C05029, doi:10.1029/2003JC001969.

Franks, P. J. S., and C. Chen (1996), Plankton production in tidal fronts: A model of Georges Bank in summer, *J. Mar. Res.*, *54*, 631–651.

Franks, P. J. S., and C. Chen (2001), A 3-D prognostic numerical model study of the Georges Bank ecosystem. Part II: Biological-physical model, *Deep Sea Res., II*, *48*, 457–482.

Houghton, R. W. (2002), Diapycnal flow through a tidal front: A dye tracer study on Georges Bank, *J. Mar. Sys.*, *37*, 31–46.

Loder, J. W., and D. G. Wright (1985), Tidal rectification and front circulation on the sides of Georges Bank, *J. Mar. Res.*, *43*, 581–604.

Loder, J. W., Y. Shen, and H. Ridderinkhof (1997), Characterization of three dimensional Lagrangian circulation associated with tidal rectification over a submarine bank, *J. Phys. Oceanogr.*, *27*, 1729–1742.

Mellor, G. L., and T. Yamada (1982), Development of a turbulence closure model for geophysical fluid problem, *Rev. Geophys. Space Phys.*, *20*, 851–875.

Naimie, C. E. (1996), Georges Bank residual circulation during weak and strong stratification periods: Prognostic numerical model results, *J. Geophys. Res.*, *101*(C3), 6469–6486.

Naimie, C. E., J. W. Loder, and D. R. Lynch (1994), Seasonal variation of the 3-D residual circulation on Georges Bank, *J. Geophys. Res.*, *99*, 15967–15989.

Pringle, J. M., and P. J. S. Franks (2001), Asymmetric mixing transport: A horizontal transport mechanism for sinking plankton and sediment in tidal flows, *Limnol. Oceanogr.*, *46*, 381–391.

Proehl, J., D. R. Lynch, D. J. McGillicuddy, and J. R. Ledwell (2005), Modeling turbulent dispersion on the north flank of Georges Bank using Lagrangian particle methods, *Cont. Shelf Res.*, *25*, 875–900.

Smagorinsky, J. (1963), General circulation experiments with the primitive equations, I. The basic experiment, *Mon. Weather Rev.*, *91*, 99–164.

Townsend, D. W., and A. C. Thomas (2002), Springtime nutrient and phytoplankton dynamics on Georges Bank, *Mar. Ecol. Prog. Ser.*, *228*, 57–74.

R. C. Beardsley, Department of Physical Oceanography, Woods Hole Oceanographic Institution, Woods Hole, MA 02543, USA.

C. Chen and Q. Xu, Department of Fisheries Oceanography, School for Marine Science and Technology, University of Massachusetts-Dartmouth, New Bedford, MA 02744, USA. (c1chen@umassd.edu)

R. Houghton, Lamont Doherty Earth Observatory of Columbia University, Palisades, NY 10964, USA.